AIAA JOURNAL
Vol. 35, No. 12, December 1997

Measurements in Rollup Region of the Tip Vortex from a Rectangular Wing

B. R. Ramaprian* and Youxin Zheng†
Washington State University, Pullman, Washington 99164-2920

The evolving three-dimensional flowfield of the tip vortex in the near wake of a rectangular wing at incidence was studied in detail, using three-component laser Doppler velocimetry. The flow quantities measured were the three components of the instantaneous velocity. These data were used to obtain the distributions of velocity, vorticity, and circulation across the vortex at several axial locations in the flow for several angles of incidence. The data have been used to understand the process of rollup of the shear layer into the vortex in the near wake, as well as its kinematic structure. The data indicate that the rollup takes place quite quickly and the inner part of the three-dimensional vortex becomes nearly axisymmetric within a distance of about two chord lengths downstream of the trailing edge. Even though the vortex behavior in the near wake is, in general, strongly dependent on the initial conditions, the vortex trajectory appears to be described reasonably well by the overall wing lift and the freestream velocity. Also, even in the near wake, circumferentially averaged mean flow properties in the inner part of the nearly axisymmetric vortex begin to exhibit a universal structure characteristic of conceptual asymptotic trailing vortices.

Nomenclature

C_L = overall wing lift coefficient
c = wing chord
L = length scale; Eq. (2)
Re = Reynolds number, $U_\infty c/\nu$
r = radial distance from the center of vortex
r_1 = radius at maximum V_θ
U = time-mean velocity in the x direction
U_∞ = freestream velocity
V = time-mean velocity in the y direction
V_θ = time-mean velocity in the θ direction
$V_{\theta 1}$ = maximum value of V_θ
W = time-mean velocity in the z direction
x = streamwise distance measured from the trailing edge
x_v = distance measured from the virtual origin (assumed to be located at the leading edge)
y = spanwise coordinate measured inboard from the tip
y_0 = y coordinate of the vortex center
z = coordinate measured normal to the freestream (vertically upwards)
z_0 = z coordinate of the vortex center
α = angle of incidence
Γ = circulation around a circle of radius r in the vortex
Γ_0 = circulation scale; Eq. (1)
Γ_1 = circulation at radius r_1
ν = kinematic viscosity
ρ = density
ω_x = axial component of vorticity
ω_y = spanwise component of vorticity
ω_z = component of vorticity along the z direction

Superscript

$*$ = value normalized by L

Introduction

THE study of the near field of a wing-tip vortex has important applications in fixed and rotary wing aerodynamics. These include the computation of aerodynamic forces on wings, flowfield in the near wake of helicopter rotor blades, and three-dimensional aspects of dynamic stall of pitching/oscillating wings. Flow-visualization studies in the past have shown that in this region the shear layer coming out of the trailing edge rolls into a spiral. The spiral gets tighter as the flow proceeds downstream, eventually leading to the formation of a strong vortex, often known as the trailing vortex. Although the shear-layer rollup occurs quite fast, it takes a distance of several tens or even hundreds of wing chords downstream for this vortex to become fully developed. The fully developed turbulent trailing vortex and its mathematical counterpart, the line vortex, have been studied analytically, as well as experimentally by several researchers in the past (e.g., Hoffman and Joubert,[1] Saffman,[2] and Phillips[3]). A detailed study of the structure of the tip vortex in the range 5–30 chord lengths downstream of the leading edge of a NACA 0012 wing has recently been reported in Ref. 4. However, the initial rollup region in the near wake of the wing (e.g., within one or two chord lengths) has not been studied in equal detail. The flow in this region is highly three dimensional and exhibits strong spatial velocity gradients (and, hence, strong vorticity components), especially in the spanwise (y) and normal (z) directions. This region in which most of the shear-layer rollup occurs is also believed to be significantly affected by the details of the wing geometry.

Prior studies of the near-field flow behind rectangular wing tips consist of both smoke visualization experiments[5–7] and quantitative studies.[8–13] Chigier and Corsiglia[8] and Corsiglia et al.[9] used a three-sensor, hot-wire probe carried on a rapidly rotating arm to measure the mean velocity components in the tip vortex in the wake extending up to 1.7 chord lengths. Francis and Kennedy[10] measured velocities in the flow region around the wing, using an x-wire probe. These measurements were not extended in to the wake. Green and Acosta[11] studied the unsteady nature of the flow in the trailing vortex, using non-intrusive double-pulsed holography in a water tunnel. They reported results for two downstream distances of 2 and 10 chord lengths. McAlister and Takahashi[12] also used nonintrusive two-component laser Doppler velocimetry (LDV) to measure the mean velocities in the vortex in the region $0.1c$–$13c$ in the wake of a rectangular wing of NACA 0015 profile. The more recent work of Dacles-Mariani et al.[13] was a combined computational and experimental exercise, which included seven-hole pitot probe measurements of the mean velocity field in the vortex over a NACA 0012 wing tip and extending to about $0.7c$ downstream of the tip, in the near wake.

In the study described in the present paper, the three-dimensional flow structure of the evolving tip vortex in the wake behind a rectangular wing of NACA 0015 profile and a semiaspect ratio of 2 has

Received Dec. 4, 1996; revision received Aug. 18, 1997; accepted for publication Sept. 14, 1997.

*Professor, School of Mechanical and Materials Engineering. Member AIAA.
†Graduate Student, School of Mechanical and Materials Engineering.

been measured using three-component LDV. These data have been obtained in the range $0.16 < x/c < 3.33$. The main features of the experiments are the use of nonintrusive instrumentation, measurement of all three of the instantaneous components of velocity, and a very high spatial density of data points that allows one to evaluate the three components of vorticity in the flowfield with acceptable accuracy. Additionally, it covers the entire region where most of the rollup takes place and where significant three dimensionality exists. Some selected results of measurements are presented and discussed. The complete set of data obtained in the present experiments has been archived on tape and is available to any interested reader.

Experimental Setup and Procedure

The experiments were conducted in a low-speed wind tunnel of 1×1 m rectangular test section. The model tested was a rectangular wing of NACA 0015 profile with a chord of 30 cm and a semispan of 60 cm. It had a square tip. The wing was mounted as a cantilever from one of the tunnel side walls, with its span horizontal as shown in Fig. 1a. The wing mounting was such that it could be pivoted about its quarter-chord axis by a dc motor and scotch-yoke mechanism. This design allowed the wing to be oscillated, if desired, about this axis in later experiments. In the present experiments, however, the arrangement was used to pitch the wing to the desired angle of incidence, where it was rigidly clamped. Water particles from an ultrasonic humidifier were used for seeding the flow so that LDV measurements could be made. These particles were introduced from a set of perforations located on the inboard half of the pressure side of the wing surface and along the tip, as shown in Fig. 1b. Because the wind tunnel exhausted through a diffuser, there was a slight negative pressure at the test section. This allowed the injection of the particles from the humidifier into the pressure side of the wing without the need for any external forcing. Preliminary tests indicated that, although there was no significant influence of the exact number and location of the seed-introduction points on the results obtained, the arrangement shown in Fig. 1b provided the best data rate for the LDV measurements. Because of the continuous evaporation of the seed particles along the stream, their size distribution changed from one station to another. The size distribution could not be measured in situ. The only test that was made to ensure that the particles followed the flow satisfactorily was to compare the results obtained for the axial velocity at a station very near the trailing edge (where the particle size was expected to be the largest) with the results from a single-sensor hot wire. These comparisons showed that the two results were within 2% of each other. These hot-wire measurements also indicate no significant effect of particle injection on the flow in the wake.

A three-component, three-color, six-beam, fiber-optic-based LDV system was used in the backscatter mode to obtain the three components of velocities in the flowfield within a focal volume of $0.2 \times 0.1 \times 0.1$ mm. Frequency shifting was used in all three channels to allow low and reverse velocities to be measured. A three-dimensional automated traverse was used to position the measuring volume of the LDV. The Doppler signals were processed by three frequency counters, whose outputs were tested for coincidence within a prescribed window of 0.5 ms before recording on computer disk. These outputs were processed subsequently to obtain the three velocity components in the tunnel coordinate system (x streamwise, y inboard, and z vertically upward, with the origin at the tip

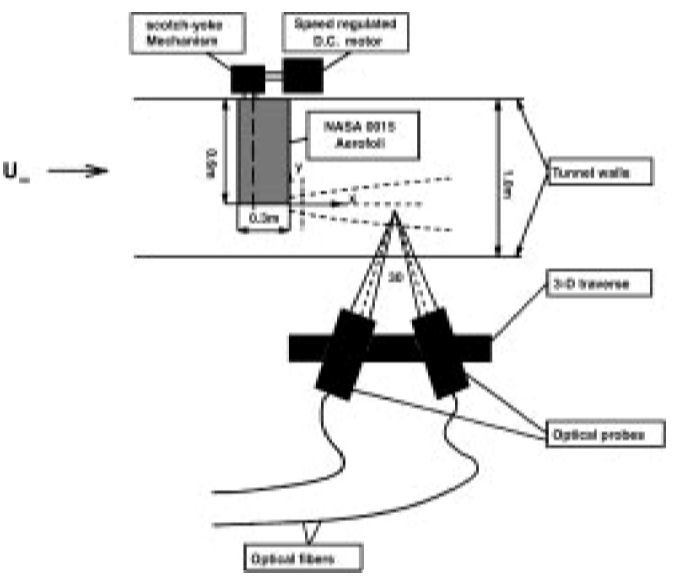

a) Wing mounting

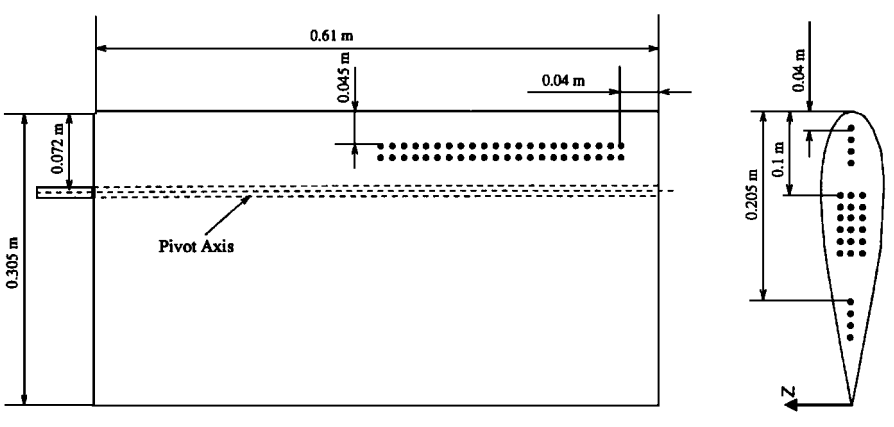

b) Wing details

Fig. 1 Schematic of the experimental setup.

of the trailing edge). No corrections for sampling bias were made because some preliminary checks (made using the interdata time information) showed that these effects were not significant in the vortex. Mean flow properties at each probe location were evaluated from averaging instantaneous velocities over about 1500 samples of data over a period of about 30–120 s (depending on the location of the point in the vortex). The three mean vorticity components at each probe location were calculated from the three mean velocity components using first-order finite difference approximation. More details of the acquisition and processing of data are given in Refs. 14 and 15.

Experiments were conducted at a freestream velocity of about 8.0 m/s, corresponding to a Reynolds number of about 1.8×10^5. Data were obtained at 10 streamwise stations in the range $0.15 \leq x/c \leq 3.3$, at each of two angles of incidence, namely, 5 and 10 deg. In addition, data were obtained at a limited number of streamwise stations at incidences of 2 and 15 deg. Also, additional data were obtained at some closely located pairs of stations ($x = 4$, 5 and 30, 32 cm) at $\alpha = 10$ deg, so that derivatives of velocities in the x direction (required for vorticity calculation) could be calculated accurately. However, the actual data indicated that the velocity gradients in the x direction were negligible compared to the gradients in the cross-stream direction. Hence, the longitudinal velocity gradients were ignored in the subsequent vorticity calculations. At each x station, data were obtained across the vortex (in the y–z plane) at about 500 points, which formed a fine grid. The size of the grid was 0.25×0.25 cm in the inner part and 0.5×0.5 cm in the outer part. Probe positioning and data acquisition were fully automated during the experiments. No major difficulties were experienced with regard to the seeding of the flow. In fact, the seeding technique used allowed the experiments to be continued with no interruption over long periods of time (typically, 10–12 h) without polluting the laboratory.

Before presenting the results, it is necessary to make some comments about the experimental limitations and uncertainties. The model size selected was a compromise between several conflicting requirements of aspect ratio and tunnel blockage on the one hand and satisfactory seeding and sensitivity and reach of the LDV on the other. With the size selected, the tunnel blockage by the wing was about 3 and 6% at incidences of 5 and 10 deg, respectively, at which most of the data were obtained. It was proportionately higher or lower at the other two incidences of 15 and 2 deg. These are conservative estimates based on a wing spanning the entire tunnel, whereas, in reality, it spanned only 67% of the tunnel width. Also, the blockage created by the wake (including the three-dimensional vortex) in the near field is considerably less than the stated estimates. The proximity of the outboard side wall (one chord length) to the wing tip might have caused some modification of the vortex trajectory, as well as its structure. A very rough estimate of the induced velocity at the vortex center due to an image vortex in the wall is about 6% of the maximum tangential velocity in the vortex. The effect of this is also to cause a lifting of the vortex trajectory by a corresponding amount. Likewise, at the relatively small aspect ratio of the model, one can expect some interaction with the corner vortex at the inboard end of the wing. It is harder to estimate this effect, but it is likely to be much smaller than the effect of the outboard wall because the inboard wall is twice as far away from the tip. It is also important to make note of two points. First, some, if not all, of these wall effects on the vortex trajectory are most likely to be accounted for by our use of the overall lift in correlating trajectory results, as shown later. Second, the side wall and blockage effects do not reduce the value of the database because the tunnel and wing geometry can be included in the computational model being developed/evaluated using these data.

The experimental uncertainties in the results reported have been estimated to be as follows: mean velocities $0.02U_\infty$ and vorticity components 15%. The velocity uncertainty quoted is based on comparison with hot-wire measurements in the wake, as already mentioned. The vorticity uncertainty estimate is based on the spatial resolution of the measurement grid used. The extent of the cross-stream region scanned in the experiments was the maximum possible that could be measured with the LDV. It was not possible to obtain any data beyond that region either because of the lack of particles or because of being outside the optical range of the LDV. Note, however, that in all cases, the measurements have captured most of the vorticity within the tip vortex. The data presented are not corrected for vortex wandering. This is not considered to be a serious shortcoming in this case. This is because these corrections are not expected to be significant in the near-field range studied in this work. This is based on rough estimates made using the model suggested in Devenport et al.[4] Furthermore, from the point of view of modeling the vortex wake in the near field, the time-averaged properties reported in this paper are of primary interest. The effects of wandering become much larger and more significant in the far field, requiring some form of conditional averaging.

Results and Discussion

Axial Velocity Contours Within the Vortex

Typical contours of the normalized mean longitudinal velocity U/U_∞ across the vortex in the region $0.16 < x/c < 3.33$ for $\alpha = 10$ deg are shown in Fig. 2. Note that only alternate contours are labeled for the sake of clarity. Also, the maximum and minimum contour values are given. It is seen that the shear layer from the wake of the wing rolls up into a spiral in the immediate near wake ($x/c = 0.33$). This spiral is associated primarily with the shear layer coming from the pressure side of the inboard region of the wing. The spiral rolls up and gets tighter as the flow moves downstream. The velocity field within the vortex is highly three dimensional in the initial region near the trailing edge. Beyond that, the low-velocity region near the vortex center tends to become more and more axisymmetric, whereas the higher-velocity outer region continues to exhibit a spiral (nonaxisymmetric) structure, as seen for $x/c = 1.67$. The velocity in this region approaches the freestream velocity beyond a distance of about $0.25c$ from the vortex center. Eventually, most of the flow in the vortex, except for the outermost part of the spiral, was found to exhibit a well-organized, near-axisymmetric pattern beyond about two chord lengths downstream from the trailing edge. This can be seen from the contours at $x/c = 3.33$. The contour values shown indicate that the velocity minimum quickly recovers from a value of 0.68 near the trailing edge to a value of about 0.74 at $x/c = 0.67$, i.e., within about 20 cm, whereas the subsequent recovery to the freestream value is very slow. In fact, at $x/c = 3.33$, it has only recovered to 0.78. It is also seen that no significant velocity excess is present within the vortex in any of the cases studied. This observation agrees with some of the reported data but contradicts some of the other reported experimental data.[11–13] However, note that, during the present experiments, the authors had no difficulty getting enough seed particles near the vortex core, unlike in some of the earlier experiments (e.g., Ref. 12). Furthermore, the absence of a velocity maximum within

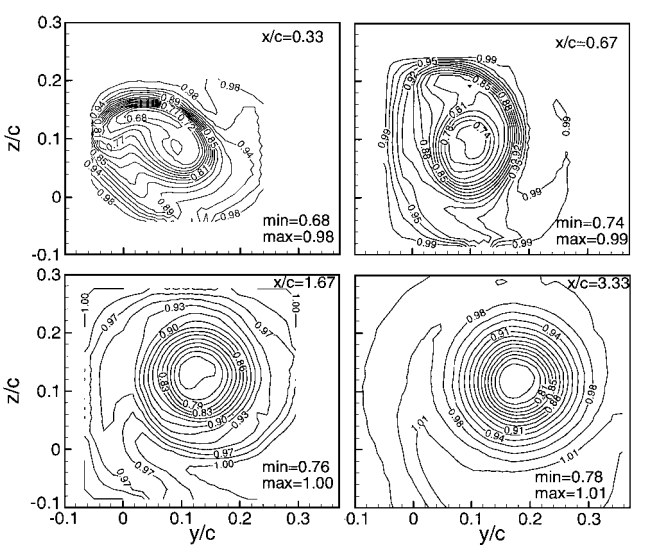

Fig. 2 Contours of normalized longitudinal velocity U/U_∞ in the tip vortex, α = 10 deg, including minimum and maximum contour values in each case. Note that only alternate contours are labeled for the sake of clarity.

the vortex has been confirmed from additional measurements made recently using a different seeding technique. The authors are, therefore, confident of the accuracy of the present experimental results. It is possible that the difference is due to the different wing loadings and/or Reynolds numbers in the two experiments (the present and that of Ref. 12), but the controversy cannot be resolved at this time.

Axial Vorticity Distribution Within the Vortex

Typical contours of the normalized axial component of the mean vorticity ($\omega_x c/U_\infty$) across the vortex in the near wake are shown in Fig. 3 for the same stations and incidence angle as in Fig. 2. The rolling up of the shear layer into the tip vortex is clearly seen from the concentration of the vorticity contours within a spiral at $x/c = 0.33$. The rollup process causes the vorticity from the shear layer leaving the trailing edge to be carried into the core region of the vortex. The rollup process is apparently very rapid, at least in terms of the vorticity distribution, because the discrete turns of the spiral can barely be identified at $x/c = 0.67$. The nearly uniform spacing of the vorticity contours in the core region of the vortex is a result of strong viscous diffusion of vorticity in that region. The magnitude of the vorticity decreases gradually from a maximum at the center to nearly zero in the outer part of the vortex. This shows that viscous/turbulent diffusion is significant in the inner part of the vortex. It is also noted that most of the vorticity is concentrated in a nearly circular area of a radius of about $0.15c$. The outer part of the vortex, i.e., the arm of the spiral, carries very little axial vorticity. After a distance of about one chord from the tip, the vorticity distributions appear to exhibit approximate axisymmetry.

As the rolling-up process continues, several competing processes determine the peak vorticity magnitude within the vortex. The first of these is the continuous trapping, by the vortex, of the vorticity from the shear layer. This tends to increase the magnitude of the maximum negative vorticity with distance. On the other hand, the second process, namely, diffusion of vorticity by viscosity and turbulence, tends to decrease the peak magnitude of the vorticity within the vortex. Other processes that may affect the evolution of the peak vorticity are vortex stretching brought about by the presence of any axial pressure gradient (causing an increase in the magnitude of peak vorticity) and the smoothening effect (reducing the peak magnitude) due to vortex wandering. The vorticity contours shown in Fig. 3 contain the combined effect of all of the preceding processes and indicate that the net result is a small but gradual increase in the magnitude of the peak negative axial vorticity within the vortex in the region $0 < x/c < 3.3$.

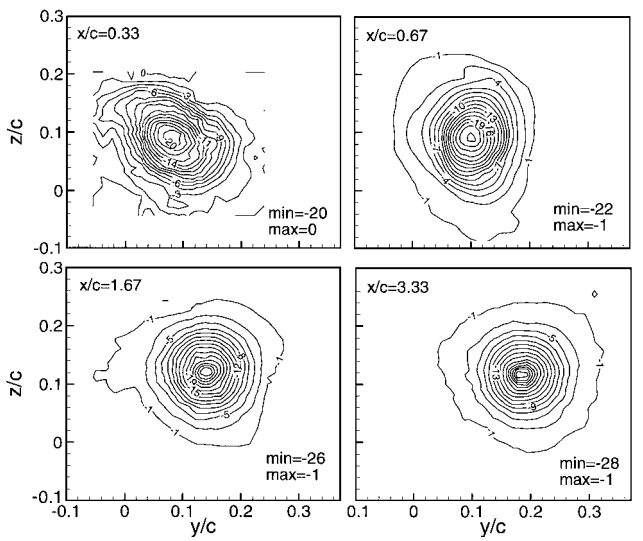

Fig. 3 Contours of normalized axial component of vorticity ($\omega_x c/U_\infty$) in the tip vortex, α = 10 deg, including minimum and maximum contour values in each case. Note that only alternate contours are labeled for the sake of clarity.

Velocity and Vorticity Vectors in the Cross-Stream Plane

Figures 4a and 4b show the mean velocity vectors ($jV + kW$) in the cross-stream plane, normalized by U_∞, at two streamwise locations for the same angle of incidence as in Figs. 2 and 3. Figures 4c and 4d show the corresponding normalized vorticity vectors ($j\omega_y + k\omega_z)c/U_\infty$. Velocity vectors are quite smooth over the entire vortex. It is also clear that there was no particular difficulty in obtaining the measurements near the vortex center. In fact, data rates up to 100 samples/s were obtained in this region. This is presumably due to the specific seed injection scheme used in these experiments. The velocity field is seen to be distinctly nonaxisymmetric at short distances from the trailing edge. However, it was found to become more nearly axisymmetric beyond $x/c = 1.0$, as can be seen from the results for $x/c = 1.67$ in Fig. 3. At all stations, the tangential velocities were generally seen to increase rapidly from almost zero at the center of the vortex to a maximum at some distance from the center, beyond which they decreased gradually along the radial direction. The reference vector shown at the top right corner in each of Figs. 4a and 4b represents the freestream velocity (of magnitude 1.0). Thus, it is seen that the maximum cross-stream velocity is often about 50% or more of the freestream velocity at both stations and is very significant. The present cross-stream velocity measurements appear to be in general agreement with the measurements of McAlister and Takahashi.[12]

The vorticity vector fields shown in Figs. 4c and 4d indicate that the shear layer coming from the trailing edge of the wing and carrying a significant amount of cross-stream vorticity rolls up into a spiral structure. As it rolls up into the core region of the vortex, the cross-stream vorticity components become small and virtually disappear near the center of the vortex. Figures 4c and 4d, along with Fig. 3, clearly indicate that the resultant vorticity vectors in the shear layer gradually rotate from a cross-stream plane into the axial direction as the rollup process continues. As a result, the axial vorticity component is augmented near the vortex center, as already noted. The reference vector shown in the top right corner of each of Figs. 4c and 4d indicates the magnitude of the peak axial vorticity at the same station (from Fig. 3). The maximum magnitude of the cross-stream vorticity vector was found to change from $0.52\omega_x$ at $x/c = 0.33$ to $0.1\omega_x$ at $x/c = 3.33$. It was also found that it was reasonable to consider ω_x as the only dominant vorticity in the vortex core region for $x/c < 3$ (as seen from Figs. 4c and 4d) and everywhere in the vortex for $x/c \geq 3$.

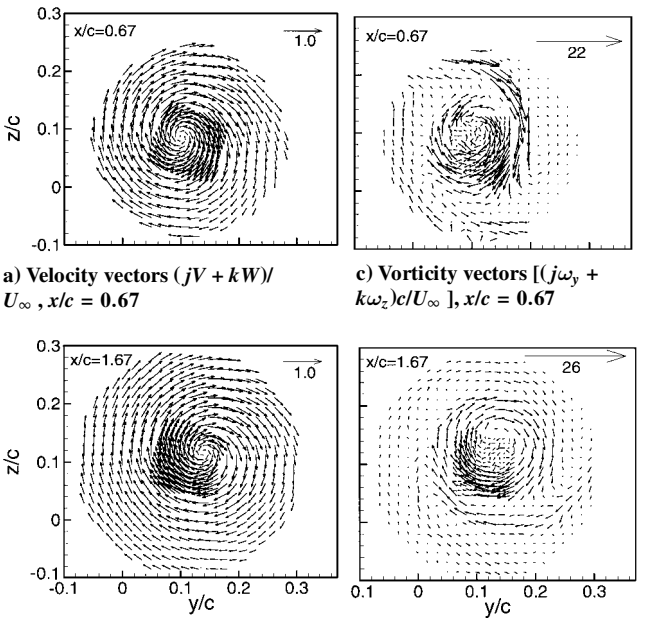

a) Velocity vectors ($jV + kW$)/ U_∞, x/c = 0.67

c) Vorticity vectors [($j\omega_y + k\omega_z)c/U_\infty$], x/c = 0.67

b) Velocity vectors ($jV + kW$)/ U_∞, x/c = 1.67

d) Vorticity vectors [($j\omega_y + k\omega_z)c/U_\infty$], x/c = 1.67

Fig. 4 Normalized velocity and vorticity vectors in the cross-stream plane in the vortex, α = 10 deg, with reference vector at top right indicating scale.

Results similar to those presented in Figs. 2–4 were also obtained at other angles of incidence. However, as the angle of incidence increases, both the wake thickness and the lift-generating circulation increase. These cause the velocity defect and vorticity magnitude to change with incidence. Also, as the incidence increases, there should be an increase in the size of the vortex because it is determined by the thickness of the shear layer that rolls up into the vortex. The data indeed indicated these trends. Also, no streamwise velocity excess was observed at any of these incidences. Details of the results at all incidences are provided in Ref. 15.

Vortex Trajectory in the Near Field

A careful study of Figs. 4a and 4b will show that the vortex center has an inboard as well as upward motion as the flow moves downstream. These motions of the vortex center in the near wake are primarily due to the continuing rollup of the shear layer arriving from the inboard regions. This rollup process causes more and more of the spanwise vorticity to be rotated into the axial direction and added to the outer layers of the tip vortex. To obtain quantitative information on the trajectory of the vortex, the vortex center (point of zero cross-stream velocity) was determined from the cross-stream velocity vector fields such as were presented typically in Figs. 4a and 4b. The estimated error in the location of the vortex center caused by the finite size of the measurement grid is less than 3 mm ($0.01c$).

In the near field, the details of the vortex structure are strongly influenced by the spanwise distribution of sectional lift, which in turn depends on the details of the wing geometry, angle of incidence, and Reynolds number. As a starting point, however, one can speculate that, except for a small distance immediately near the trailing edge, the global behavior of the vortex, as represented by its trajectory, would correlate with a single characteristic quantity such as the overall lift generated by the wing. To test this hypothesis, let us first identify, from simple phenomenological reasoning, the length, circulation, and velocity scales appropriate for describing the vortex trajectory in this region of the near field. We will use the freestream velocity U_∞ as the appropriate velocity scale. We can define an overall circulation scale Γ_0 by writing

$$\rho U_\infty \Gamma_0 = \tfrac{1}{2} C_L \rho U_\infty^2 c \tag{1}$$

and using an experimentally measured overall lift coefficient C_L. A characteristic global length scale L of the wing tip vortex can then be defined as

$$L = \Gamma_0 / U_\infty \tag{2}$$

Note that the preceding definition gives $L = cC_L/2$. The values of C_L used in Eq. (1) were obtained from the data of Szafruga and Ramaprian[16] for the same wing model in the same configuration in the tunnel.

The upward and inboard movements of the vortex center are shown in Figs. 5a and 5b, respectively, in terms of variables normalized using L as the longitudinal reference length. The streamwise coordinate x_v used for this analysis is the distance from the virtual origin of the vortex. The process of determining the virtual origin for the vortex involves trial and error and considerable ambiguity. In the present case, we found that assuming the virtual origin to be located at the leading edge of the wing is satisfactory for the study of the vortex trajectory. This assumption was also supported by observations of surface flow visualization near the wing tip. Figures 5a and 5b show the results for all of the angles of incidence. The data collapse together reasonably well, indicating that the vortex trajectory in the near field is primarily determined by the overall lift and that treating the leading edge of the wing as the virtual origin is a reasonable approximation for this purpose. Curve fits to the data in Figs. 5a and 5b yield the equations

$$y_0^* = 0.09\left(x_v^*\right)^{0.75} \tag{3}$$

and

$$z_0^* = 0.09\left(x_v^*\right)^{0.50} \tag{4}$$

These results were obtained from the data for a specific wing geometry. However, the blockage and side-wall interference effects

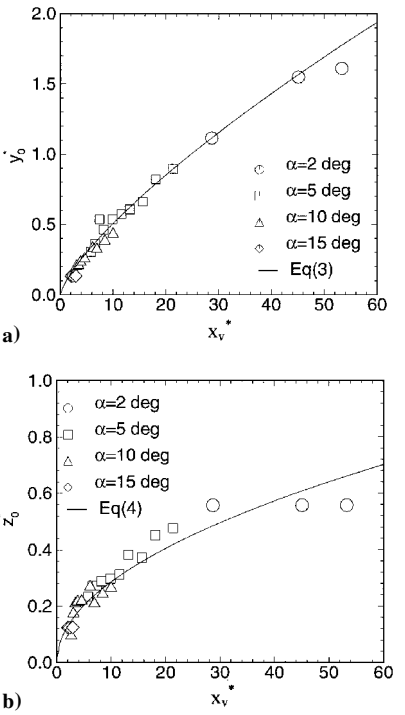

Fig. 5 Rise and inboard movement of the vortex center in the near wake.

varied with the angle of incidence during the tests. Hence, it seems safe to conclude that, within reasonable limits, the vortex trajectory in the near field for a given wing geometry can be described by Eqs. (3) and (4) even in the presence of blockage and side-wall interference effects. On the other hand, one needs more data to study the possibility of extending Eqs. (3) and (4) to other wing geometries. It is interesting that the form of Eq. (3) for the near field is not inconsistent with the trend $y_0 \propto x_v^{0.5}$ obtained for larger distances downstream of a NACA 0012 wing in Ref. 4. Note, however, that y_0 should eventually remain constant at asymptotically large distances. Equation (4) for the vortex liftoff also appears to be supported by the data of Ref. 4, even though the two sets of data cannot strictly be compared.

Approach of the Vortex Toward Asymptotic Behavior

The tip vortex in the near field soon after it is generated is highly three dimensional. As the vortex rollup continues, the spirals get tighter and tighter, but the spiral structure of the vortex continues to exist over several tens of chord length. In fact, it will never strictly attain the structure of a so-called asymptotic line vortex convected by a uniform stream. However, the present data indicates that a large inner part of the vortex rolls up quickly and that the layers of the spiral merge together to result in a nearly axisymmetric structure within about two chord lengths downstream. The characteristic features of an asymptotic viscous trailing vortex (sometimes referred to as a Q-vortex[4]) are discussed by Batchelor.[17] Squire[18] and Phillips[3] have obtained corresponding analytical descriptions of the asymptotic turbulent trailing vortex. Here, the term asymptotic is used to mean that $|(U_\infty - U)/U_\infty| \ll 1$. It is worthwhile to examine the present data on the wing-tip vortex in the near field, in the framework of the cited asymptotic theories, even though the present vortex is quite far from such an asymptotic state. For this purpose, we shall first introduce cylindrical coordinates with origin located at the vortex center and use circumferentially averaged flow properties to describe the structure of the nearly axisymmetric vortex and to study its evolution downstream.

Figure 6 shows, as a typical example, the distributions of some of the important circumferentially averaged properties (U, ω_x, Γ, and V_θ) as functions of radius, for an incidence of 5 deg and at the most downstream location measured, namely, $x/c = 3.33$. The distributions exhibit all of the qualitative features of the asymptotic viscous/turbulent vortices, such as zero tangential velocity at the

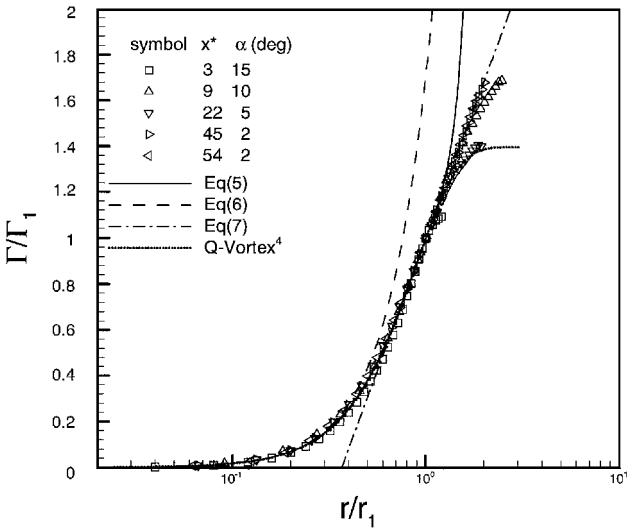

Fig. 9 Comparison of the present data from the most downstream stations with analytical and empirical asymptotic models for laminar and turbulent vortices.

by comparing this self-similar distribution with the universal distribution

$$\Gamma/\Gamma_1 = 1.7720(r/r_1)^2 - 1.0467(r/r_1)^4 + 0.2747(r/r_1)^6 \quad (5)$$

arrived at by the asymptotic analysis of the inner region of the fully merged turbulent trailing vortex in Ref. 3. It is seen that Eq. (5) is a very good description of the vortex structure in the inner region $0 < r/r_1 < 1.2$. In fact, the agreement extends to a slightly larger radial distance if the data are compared with the piecewise profiles

$$\Gamma/\Gamma_1 = 1.74(r/r_1)^2 \qquad \text{for} \qquad r/r_1 < 0.4 \quad (6)$$

$$\Gamma/\Gamma_1 = 2.14\log(r/r_1) + 1.0 \qquad \text{for} \qquad 0.5 < r/r_1 < 1.4 \quad (7)$$

arrived at by Hoffman and Joubert[1] from essentially phenomenological arguments based on a constant eddy-viscosity hypothesis. Figure 9 also shows the circulation distribution, taken from Ref. 4, in a constant-viscosity Q-vortex, be it laminar[17] or turbulent.[18] It is seen that in the range $r/r_1 < 1.2$, this distribution is indistinguishable from either Eq. (5) or the present experimental data. Factors such as Reynolds number, spanwise distribution of circulation on the wing, and whether the flow is laminar or turbulent perhaps affect only the evolution of the length and circulation (or, equivalently, the velocity) scales of the vortex.

There seems to be some controversy in the literature about the existence of a fully universal turbulent vortex state, but that discussion is outside the scope of this paper. On the other hand, the relevant important point is that the normalized mean flow structure within the inner region ($0 < r/r_1 < 1.4$) of the wing tip vortex approaches a universal structure in the near field, even though the evolution of the length and velocity scales of the vortex are still strongly dependent on the initial conditions. Reference to Fig. 6 shows that this inner region, in fact, covers an extent within which about 90% of the total variations in circulation and axial vorticity occur. The precise reason for such a quick establishment of a universal structure in this case is not known, even though such a situation is not unique for the tip vortex. For example, two-dimensional wakes and jets display near-universal velocity distributions long before these flows have reached a so-called asymptotic state. Devenport et al.[4] point out that vortex wandering alone would produce this universal structure. Whatever the reason is for the establishment of the universal structure, the fact that it exists is quite significant. This is because the calculation of the near-field vortex structure for any finite wing is now reduced to the calculation of the vortex trajectory and the two scales $r_1(x)$ and $\Gamma_1(x)$. This fact can possibly be exploited to simplify the handling of the downstream boundary conditions in the wake in the numerical computations of finite wing aerodynamics.

Conclusions

The present experiments have yielded very detailed information on the time-averaged flow structure of the wing-tip vortex in the highly three-dimensional near-wake region. The vortex core is dominated by axial vorticity, which is maximum at the center and decreases nearly to zero (due to viscous/turbulent diffusion) in the outer part of the vortex. Trajectory data for the vortex for different incidences can be collapsed together reasonably well by defining a length scale based on the overall lift coefficient. Most of the vortex, with the exception of the outermost part, becomes nearly axisymmetric beyond about two chord lengths downstream. The study of the circumferentially averaged properties in this region shows that while the length and velocity scales of the vortex continue to evolve in the near wake, the time-averaged flow structure within the inner part of the vortex quickly attains a well-known universal state. This may be significant in the modeling of the vortex wake in numerical computations of finite wing aerodynamics.

Acknowledgments

This work was performed with support from U.S. Army Research Office Grants DAAL03-87-G-0011 and DAAL03-91-G-0026 and Air Force Office of Scientific Research Grant AFOSR-90-0131. The support from these sources is gratefully acknowledged.

References

[1]Hoffman, E. R., and Joubert, P. N., "Turbulent Line Vortices," *Journal of Fluid Mechanics*, Vol. 16, Pt. 3, 1963, pp. 395–411.

[2]Saffman, P. G., "Structure of Turbulent Line Vortices," *Physics of Fluids*, Vol. 16, No. 8, 1973, pp. 1181–1188.

[3]Phillips, W. R. C., "The Turbulent Tailing Vortex During Roll-Up," *Journal of Fluid Mechanics*, Vol. 105, April 1981, pp. 451–467.

[4]Devenport, W. J., Rife, M. C., Liapis, S. I., and Follin, G. J., "The Structure and Development of a Wing-Tip Vortex," *Journal of Fluid Mechanics*, Vol. 312, April 1996, pp. 67–106.

[5]Francis, T. B., and Katz, J., "Observations on the Development of a Tip Vortex on a Rectangular Hydrofoil," *Journal of Fluids Engineering*, Vol. 110, No. 2, 1988, pp. 208–215.

[6]Freymuth, P., "Three-Dimensional Vortex Systems of Finite Wings," *Journal of Aircraft*, Vol. 25, No. 4, 1988, pp. 971, 972.

[7]Liang, X., and Ramaprian, B. R., "Visualization of the Wing–Tip Vortex in Temporal and Spatial Pressure Gradient," *Journal of Fluids Engineering*, Vol. 113, No. 3, 1991, pp. 511–515.

[8]Chigier, N. A., and Corsiglia, V. R., "Tip Vortices—Velocity Distributions," NASA TM X-62087, Sept. 1971.

[9]Corsiglia, V. R., Schwind, R. K., and Chigier, N. A., "Rapid Scanning Three Dimensional Hot Wire Anemometer Surveys of Wing-Tip Vortices," *Journal of Aircraft*, Vol. 10, No. 12, 1973, pp. 752–757.

[10]Francis, M. S., and Kennedy, D. A., "Formation of a Trailing Vortex," *Journal of Aircraft*, Vol. 16, No. 3, 1979, pp. 148–154.

[11]Green, S. I., and Acosta, A. J., "Unsteady Flow in Trailing Vortices," *Journal of Fluid Mechanics*, Vol. 227, June 1991, pp. 107–134.

[12]McAlister, K. W., and Takahashi, R. K., "Wing Pressure and Trailing Vortex Measurements," NASA TP 3151, Nov. 1991.

[13]Dacles-Mariani, J., Zilliac, G. G., Chow, J. S., and Bradshaw, P., "Numerical/Experimental Study of a Wingtip Vortex in the Near Field," *AIAA Journal*, Vol. 33, No. 9, 1995, pp. 1561–1569.

[14]Zheng, Y., and Ramaprian, B. R., "LDV Measurements in the Roll-Up Region of the Tip Vortex from a Rectangular Wing," AIAA Paper 91-1685, June 1991.

[15]Zheng, Y., and Ramaprian, B. R., "An Experimental Study of the Wing Tip Vortex in the Near Wake of a Rectangular Wing," Dept. of Mechanical Engineering, Rept. MME-TF-93-1, Washington State Univ., Pullman, WA, June 1993.

[16]Szafruga, J., and Ramaprian, B. R., "Pressure Measurements over the Tip Region of a Rectangular Wing, Part I. Stationary Wing," AIAA Paper 94-1948, June 1994.

[17]Batchelor, G. K., "Axial Flow in Trailing Vortices," *Journal of Fluid Mechanics*, Vol. 20, Pt. 4, 1964, pp. 645–658.

[18]Squire, H. B., "The Growth of a Vortex in Turbulent Flow," *Aeronautical Quarterly*, Vol. 16, 1965, pp. 302–306.

A. Plotkin
Associate Editor